

## Supporting information for

# Terahertz Time-Domain Spectroscopy of thermoresponsive polymers in aqueous solutions.

*Guillaume Serin<sup>†,‡</sup>, Hong Hanh Nguyen<sup>‡</sup>, Jean-Daniel Marty<sup>‡</sup>, Jean-Claude Micheau<sup>‡</sup>, Véronique Gernigon<sup>‡</sup>, Anne-Françoise Mingotaud<sup>‡</sup>, Damienne Bajon<sup>†</sup>, Thierry Soulet<sup>†</sup>, Sébastien Massenet<sup>\*,†</sup>, Christophe Coudret<sup>\*,‡</sup>*

<sup>†</sup> Institut Supérieur de l'Aéronautique et de l'Espace (ISAE-SUPAERO), Université de Toulouse, 31055 Toulouse Cedex 4, France.

<sup>‡</sup> Laboratoire des IMRCP, Université de Toulouse, CNRS UMR 5623, Université Paul Sabatier, 118 route de Narbonne 31062 Toulouse Cedex 9, France

CONTENT :

S1. POLYMER CHARACTERIZATION.....	3
S2. PARAMETER EXTRACTION FOR TERAHERTZ TIME-DOMAIN SPECTROSCOPY.....	4
S3. VALIDATION OF THE SETUP: MEASUREMENT OF ABSORPTION COEFFICIENT OF PURE LIQUID WATER. ....	6
S4. CLOUD POINT TEMPERATURE MEASUREMENT OF HIGHLY CONCENTRATED SAMPLES.....	7
S4.1. Terahertz Time-Domain Spectroscopy. ....	7
S4.2. Differential Scanning Calorimetry.....	9

S4.3. Turbidimetry .....	13
S4.4. Dynamic Light Scattering .....	14
S5. METHODOLOGY TO CALCULATE THE SOLVATION WATER ABSORPTION COEFFICIENT $\alpha^S$ .....	15
S6. EXTRACTION OF THE COIL-TO-GLOBULE $r(T)$ WITH NUMERICAL METHOD $r(T)$ .....	17
S6.1. Vant'Hoff plots .....	17
S6.2. $r(T)$ formula.....	19
S7. SUPPLEMENTARY REFERENCES .....	23

### **Corresponding authors**

\*C. Coudret: tel (+33) (0)5 61 55 62 75; fax (+33) (0)5 61 55 62 75; e-mail: [coudret@chimie.ups-tlse.fr](mailto:coudret@chimie.ups-tlse.fr)

\*S. Massenot: tel (+33) (0)5 61 33 80 77; e-mail: [sebastien.massenot@isae-supero.fr](mailto:sebastien.massenot@isae-supero.fr)

## S1. POLYMER CHARACTERIZATION

The average molecular weights of the PNIPAm samples were determined by Size Exclusion Chromatography (SEC) as well as their polydispersity index (PDI) for P2k and P7k. The apparatus was equipped with a Waters 2140 refractive index (RI) detector, using a Waters Styragel HR 4E column (eluent, THF, flow rate, 1 mL.min<sup>-1</sup>). Samples of concentration 5 mg.ml<sup>-1</sup> were injected. Alternatively, samples were analyzed with a SEC apparatus comprising a Varian ProStar 325 UV detector (dual wavelength analysis) and a Waters 410 refractive index detector using two Shodex K-805 L columns (8 mm, 300 mm, 12 μm) and DMF LiCl (1 g.L<sup>-1</sup>) as the eluent at 40°C (flow rate, 1 mL.min<sup>-1</sup>).

## S2. PARAMETER EXTRACTION FOR TERAHERTZ TIME-DOMAIN SPECTROSCOPY

Two THz pulses, proportional to the wave electric field, are recorded, one as a reference with an empty capillary tube and one as sample data with a filled capillary tube. Time-Domain signals are truncated to remove peaks due to Fabry-Perot reflections at the quartz-air interfaces (figure S2.1a). In addition, such reflections are not predominant due to the high absorption coefficient of water. Then, a Blackman window is applied to provide antialiasing effect before treating the time-domain data (figure S2.1b).

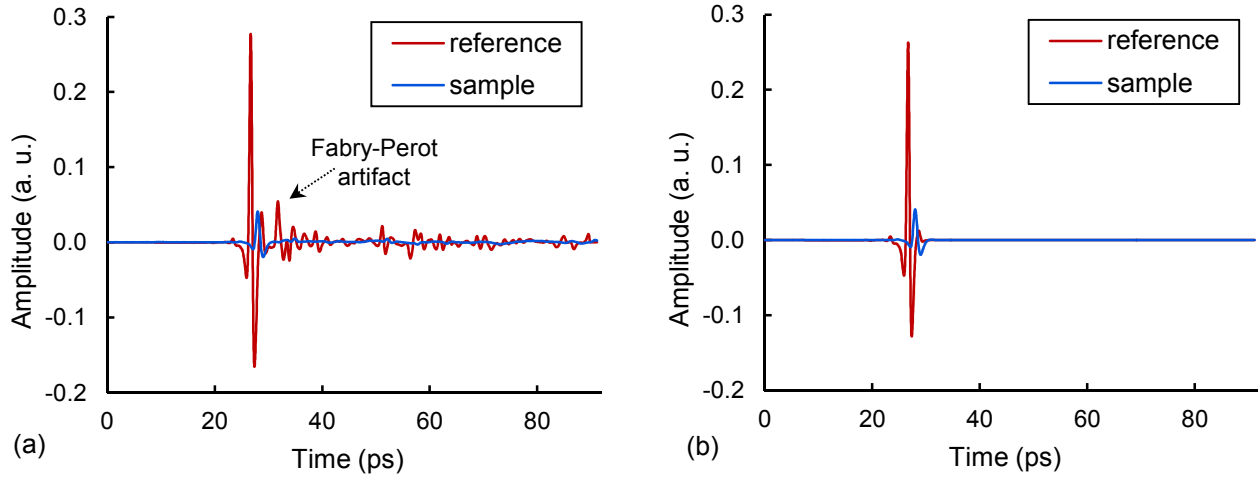


**Figure S1.** Signal processing of the time-domain pulses: a) Time-domain signal and b) Truncated Blackman windowed time-domain signal.

Both pulses are then Fast Fourier-transformed (FFT) to process the signal in the frequency domain  $f$  (figure S2.2.). Their amplitudes ( $E_{\text{ref}}(f)$ ,  $E_{\text{sample}}(f)$ ) and their phases ( $\Phi_{\text{ref}}(f)$ ,  $\Phi_{\text{sample}}(f)$ ) are used to extract the refractive index  $n(f)$  and absorption coefficient  $\alpha(f)$ . Formulas S2.1-3<sup>1</sup> below show how to get these data with a single-pass (no Fabry-Perot reflections) plane waves model (phases are taken positive in the refractive index formula).

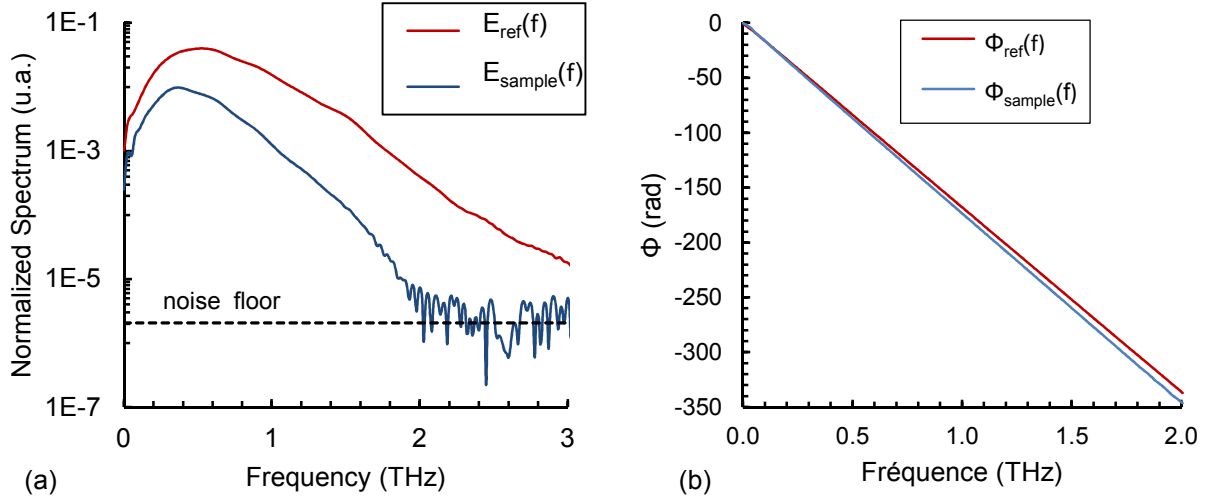


**Figure S2.** a) FFT-Amplitude and b) FFT-phases of reference and sample time domain signals.

$$n(f) = 1 + c \left( \frac{\Phi_{\text{sample}}(f) - \Phi_{\text{ref}}(f)}{2\pi f d} \right) \quad (\text{S2.1})$$

$$T(f) = 1 - \frac{[n(f) - 1]^2}{[n(f) + 1]^2} \quad (\text{S2.2})$$

$$\alpha(f) = - \ln \left( \frac{T(f) E_{\text{sample}}(f)}{E_{\text{ref}}(f)} \right) \cdot \frac{1}{d} \quad (\text{S2.3})$$

Where  $T$  is the transmission coefficient of the sample and  $d$  is its thickness. In this study, we only used the values between 0.3 and 1.5 THz or less to have a reasonable signal-to-noise ratio.

S3. VALIDATION OF THE SETUP: MEASUREMENT OF ABSORPTION COEFFICIENT OF PURE LIQUID WATER.

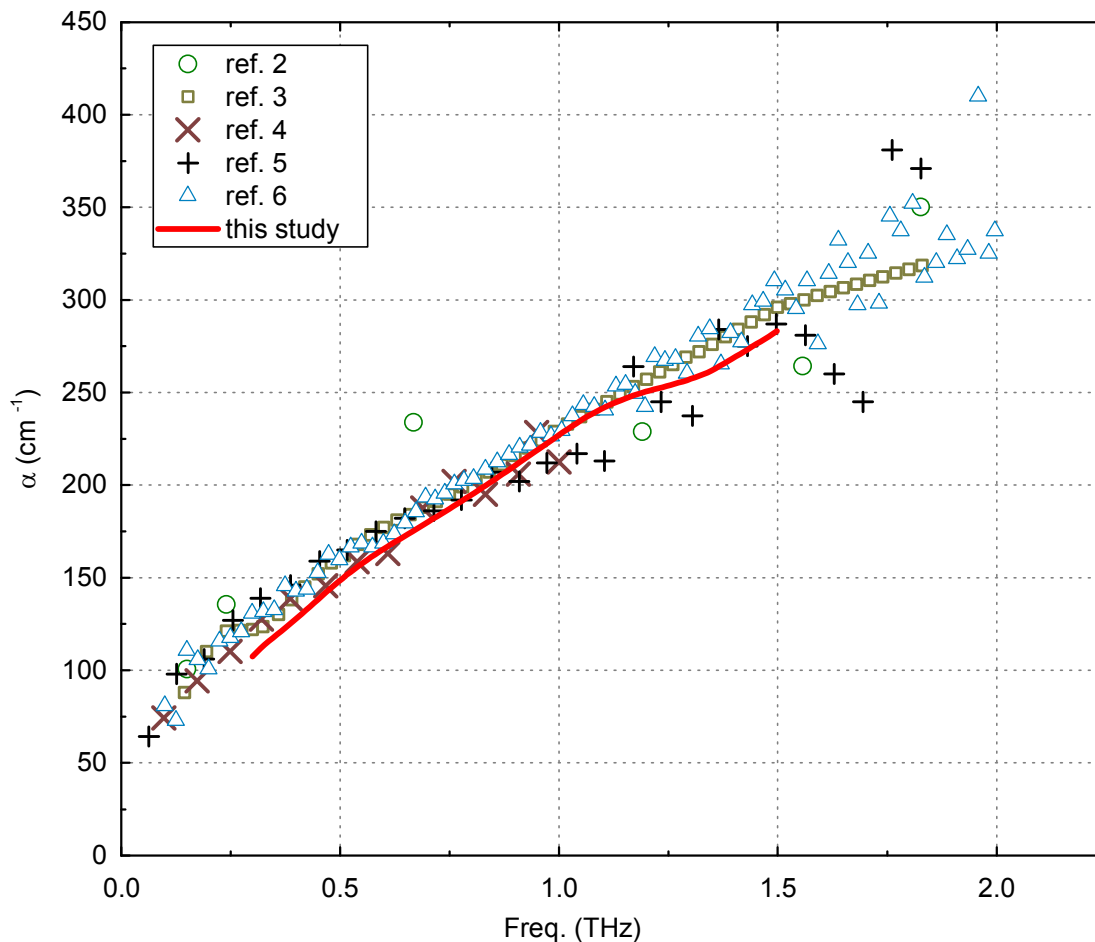


**Figure S3.** Comparison of different absorption spectra of liquid distilled water at T=20°C.

With  $\bullet$  Far Infrared laser results from Vij et Hufnagel,<sup>2</sup>  $\square$  Fourier-Transform FIR results from Hasted et al.,<sup>3</sup>  $\times$  THz pulse reflection results from Thrane et al.,<sup>4</sup>  $+$  THz-TDS results from Kindt and Schmuttenmaer,<sup>5</sup>  $\triangle$  THz reflection spectroscopy from Rønne et al.,<sup>6</sup> and red solid line is our results by THz-TDS. This comparison is adapted from ref. 5.

## S4. CLOUD POINT TEMPERATURE MEASUREMENT OF HIGHLY CONCENTRATED SAMPLES

### S4.1. Terahertz Time-Domain Spectroscopy.

For each sample presented in this study, the sample was first heated then cooled following the temperature programs shown below to observe the phase transition in THz-TDS (figure S4.1.1).

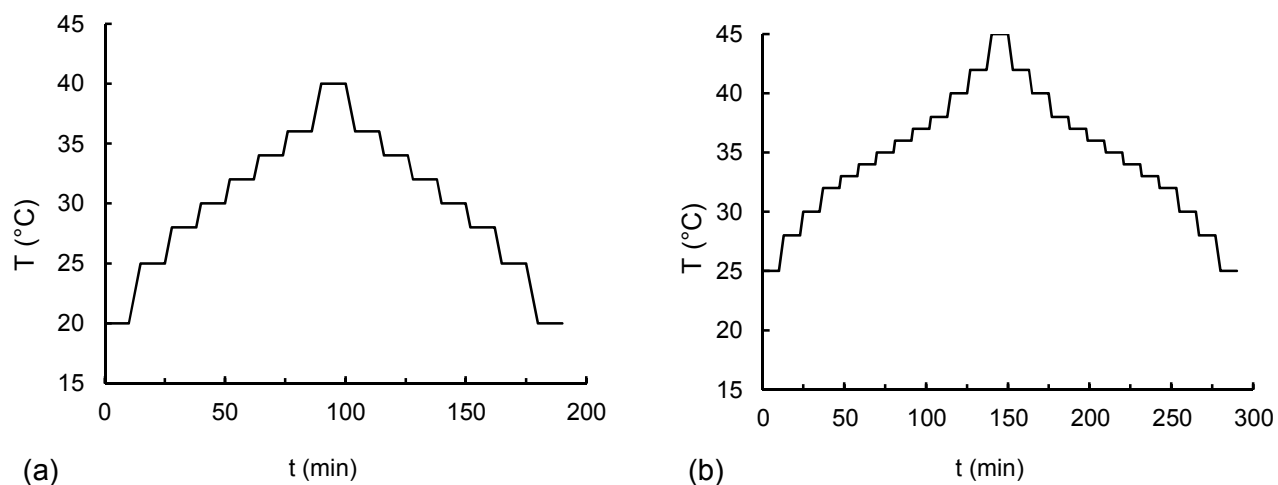


**Figure S4.** Heating-Cooling cycle performed with a) PNIPAm samples and b) PVCL samples. As previously mentioned in Temperature Control section, 10 minutes plateaus are necessary to measure 3 time-domain pulses per experimental data point.

We obtained sigmoidal curves (figure S4.1.2), from which we extracted the cloud point temperature for both heating and cooling process. The determination of the cloud temperature  $T_c$  is given by the maximum value of the first derivative of the interpolated curves (figure S4.1.3). As expected,  $T_c$  is independent from the frequency of observation.

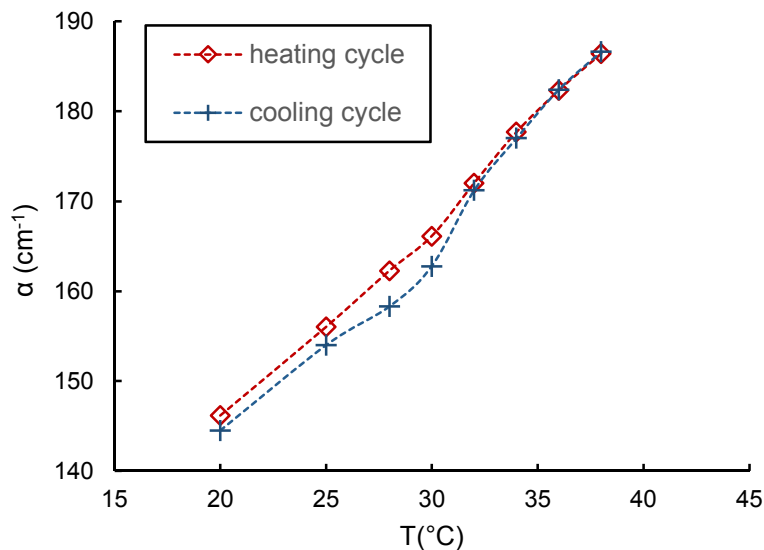


**Figure S5.** Hysteresis exhibited between the heating and the cooling of the sample P20K15 at 0.8 THz. A different cloud point was calculated for each process with the derivative of interpolated curves (dotted lines) from data measurements (red diamonds and blue crosses).

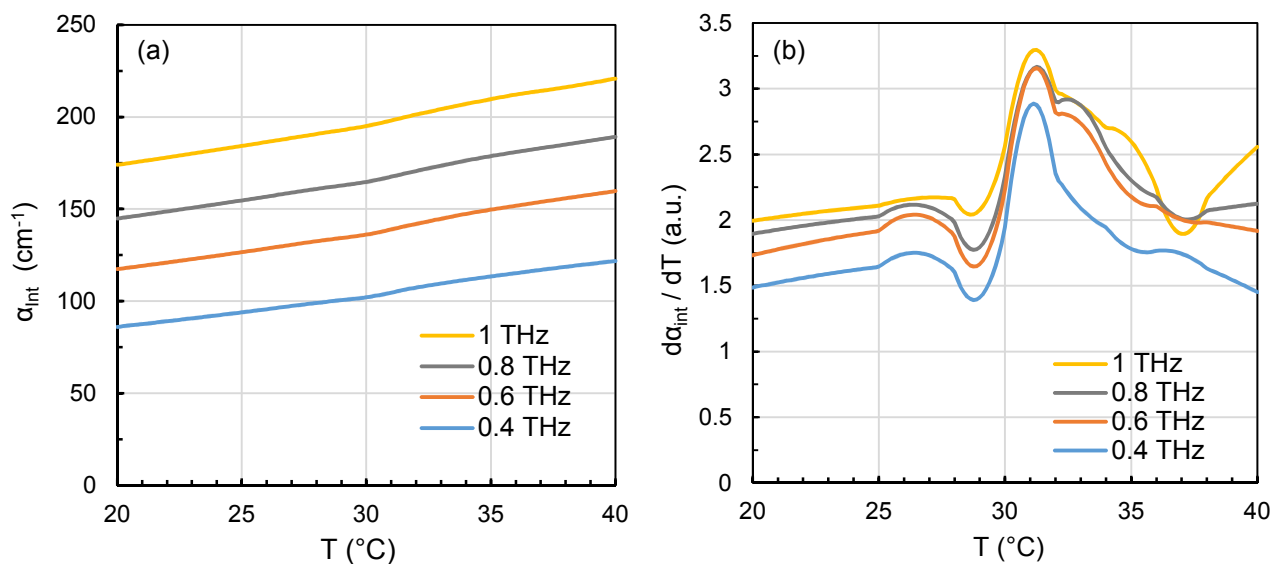


**Figure S6.** a) Interpolated values  $\alpha_{\text{int}}$  obtained from experimental data of sample P20K15 at four frequencies chosen for the illustration; b) derivatives of the interpolated curves  $\alpha_{\text{int}}$ , in each of the four examples we interpreted the maxima of these derivatives to be the cloud point temperature  $T_c$ .

## S4.2. Differential Scanning Calorimetry.

Differential Scanning Calorimetry measurements were obtained with a Mettler Toledo DSC 1 STARe System Thermal Analysis calorimeter. Samples were weighed then encapsulated in aluminum 120  $\mu\text{L}$  hermetic crucibles. Thermograms were taken with heating rates from  $1^\circ\text{C}/\text{min}$  to  $5^\circ\text{C}/\text{min}$ , with a temperature range from  $-5$  to  $90^\circ\text{C}$  (figure S7).

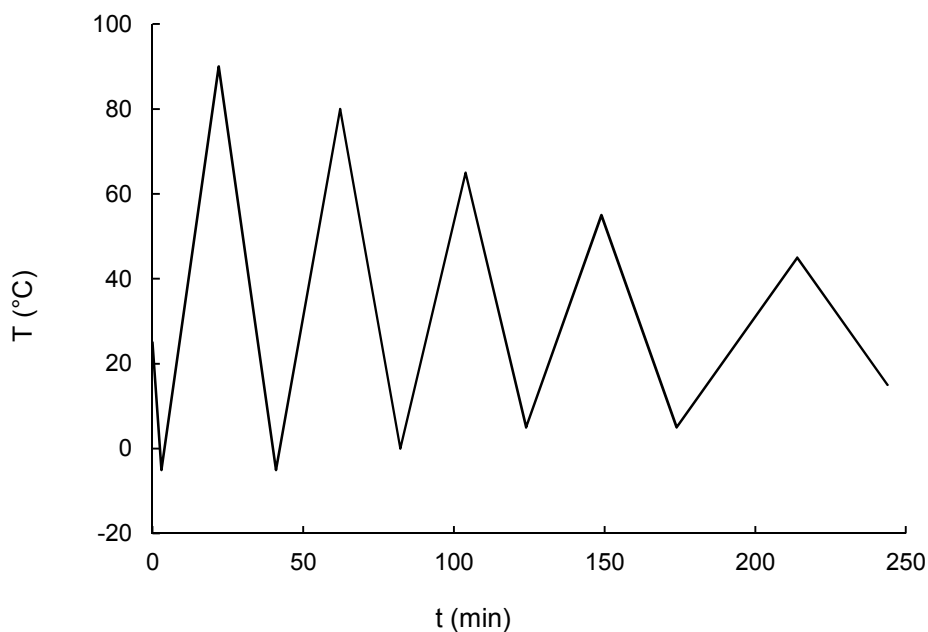


**Figure S7** Heating-Cooling cycles used for PNIPAm 2k, 7k, 20k.

For each sample, our methodology was to plot the top of DSC peaks at different heating rates, then an extrapolation determines the transition temperature at  $0^\circ\text{C}/\text{min}$ , which gives the LCST value (Figure S8 and S9).

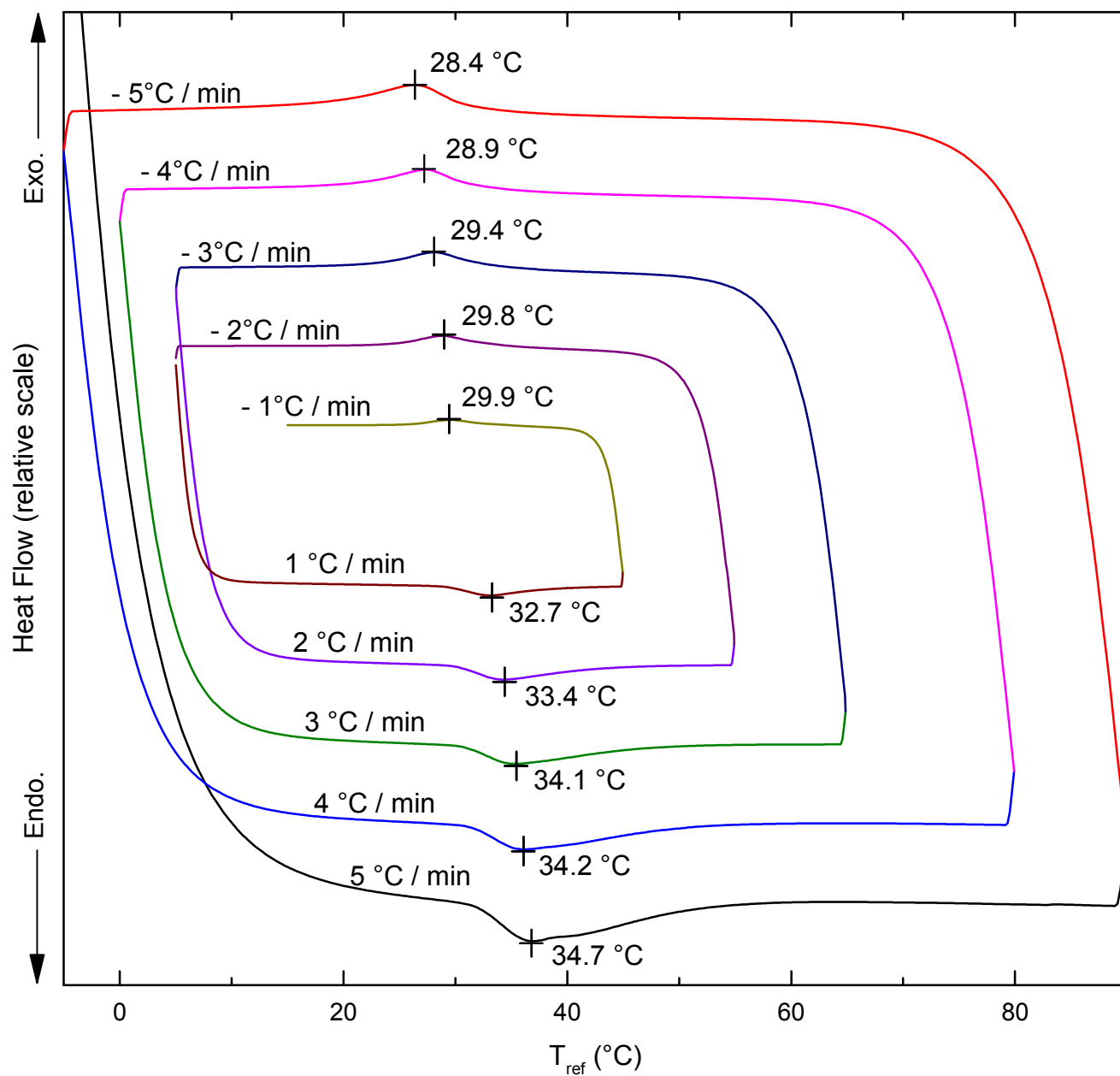


**Figure S8.** Complete thermogram analysis of P7K15 sample in function of reference temperature.

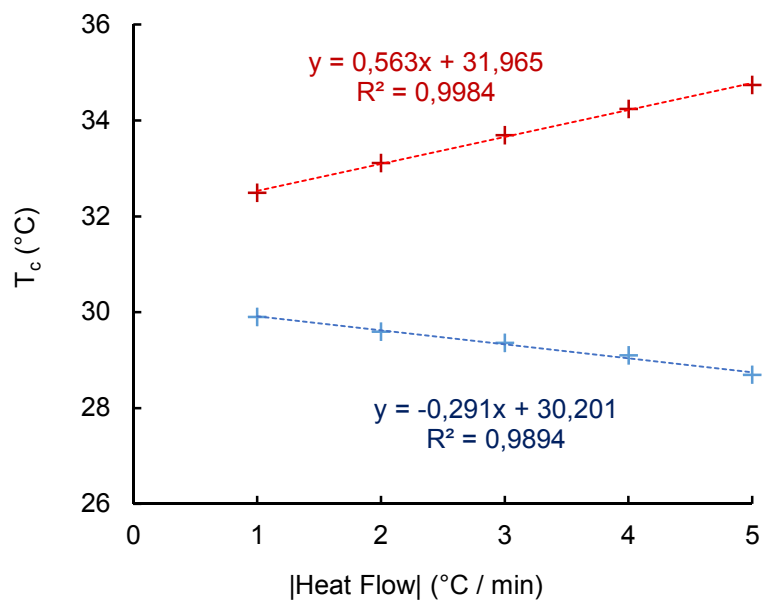


**Figure S9.** Extrapolation method for cloud point determination by DSC: the equation of the trending curve (dashed lines) calculated from the data (crosses) gives  $T_c$  for a heating rate of  $0^\circ\text{C}/\text{min}$ . This data were obtained with a sample P7K15. Here, the LCST is  $32.0^\circ\text{C}$  for the heating process in red, and  $30.2^\circ\text{C}$  for the cooling process in blue.

**Table S1.** Cloud temperature measurements comparison between THZ-TDS and DSC for heating and cooling processes.

Sample name	Tc from THZ-TDS measurements (°C)		Tc from DSC measurements (°C)	
	Heating process	Cooling process	Heating process	Cooling process
P2k20	31.1	28.8	30.8	28.7
P7k5	31.1	29.2	32.1	30.4
P7k10	31.2	30.8	32.7	30.2
P7k15	31.1	31.0	32.3	30.6
P7k20	31.2	30.8	31.7	30.3
P20k5	32.9	31.1	32.2	32.6
P20k10	29.0	32.9	33.1	32.7
P20k15	31.3	31.1	33.5	33.2
P20k20	31.3	31.1	32.9	31.4
PVCL60k20	36.4	34.6	36.1	35.5
PVCL60k1	35.5	35.5	33.8	-

### S4.3. Turbidimetry

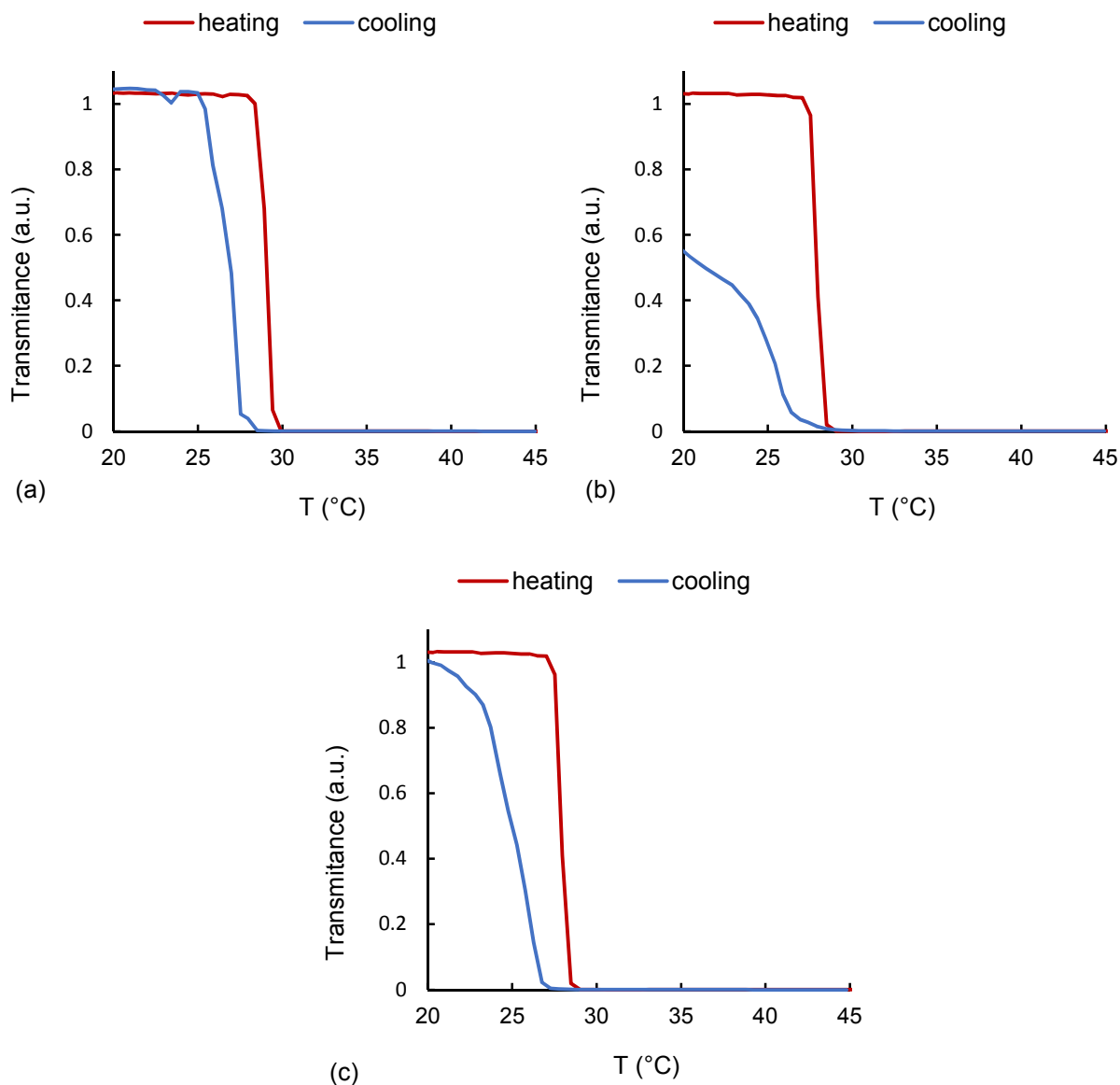


**Figure S10** Transmittance monitored at 500nm as a function of temperature for samples a) P7K5 b) P7K10 and c) P7K15. Every solution was stirred, the heating rate was  $1^{\circ}\text{C}\cdot\text{min}^{-1}$ . The demixing process of the concentrated samples made this technique difficult to perform, especially the monitoring of the cooling process.

#### S4.4. Dynamic Light Scattering

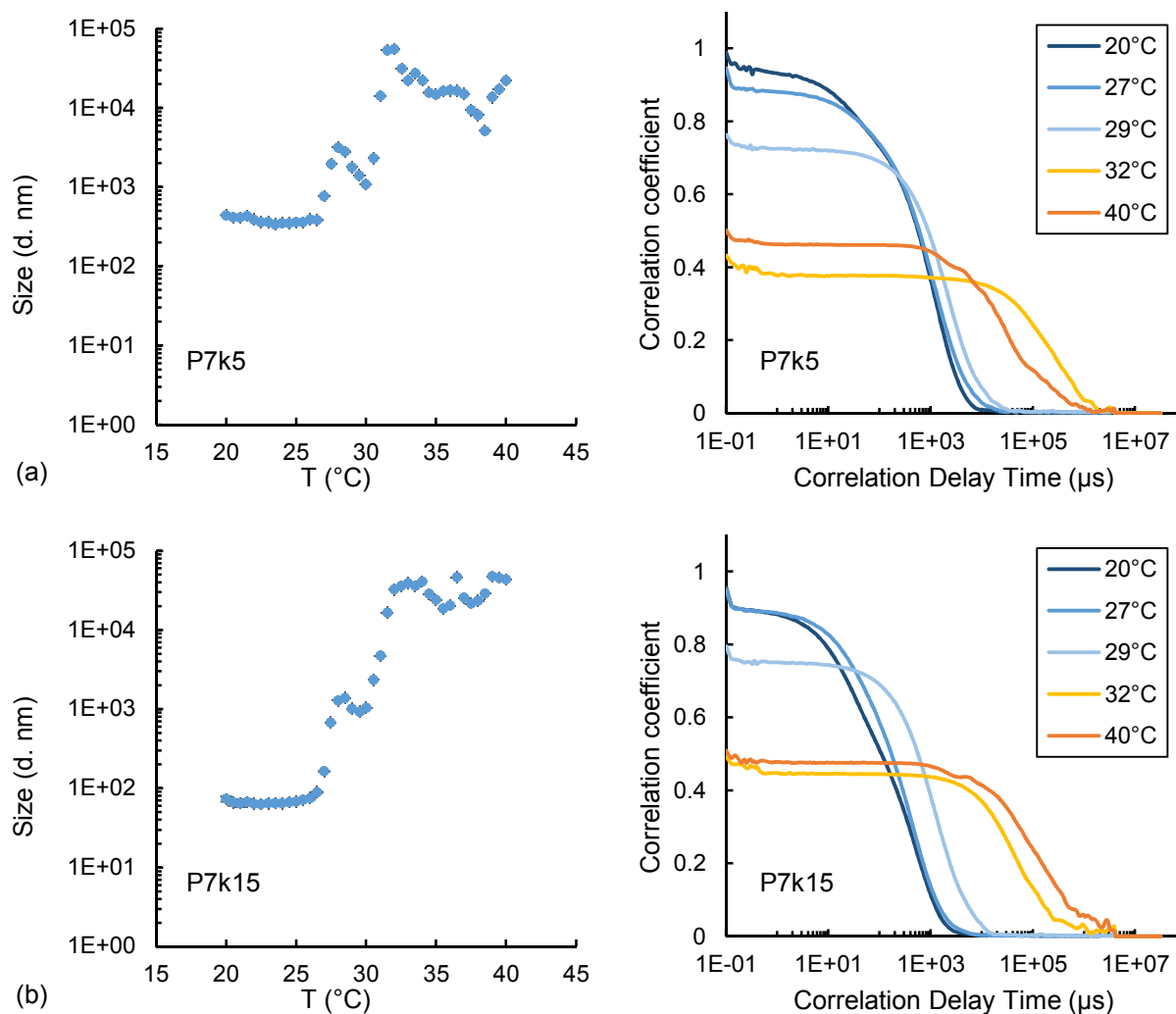


**Figure S11** Size intensity distribution and their correlograms measured by Dynamic Light Scattering for a) P7K5 and b) P7K15. Here, the results do not provide clear information on the cloud point temperature, due to sedimentation during the demixing process.

## S5. METHODOLOGY TO CALCULATE THE SOLVATION WATER ABSORPTION COEFFICIENT $\alpha^s$

We calculated the solvation water absorption coefficient at temperatures 20, 25 and 28°C, based on the literature to choose a value of the hydration number when the polymer is hydrophilic (figure S12).

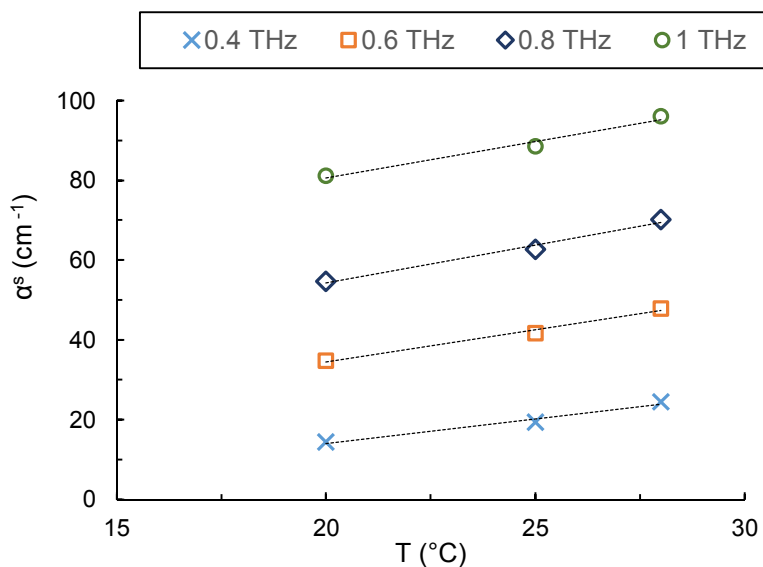


**Figure S12.** Estimation of the solvation water absorption coefficient with the hypothesis  $N_h=11$  for sample P7K15. Lines are guides for the eyes.

We extrapolated the solvation water absorption coefficient at  $T > 28^\circ\text{C}$  by assuming a linear behavior, similar to the one of pure liquid water. These results (figure S13) lead us to the calculation of the mass fraction of the solvation water (eq. 9), and to the calculation of the hydration number (eq. 10).

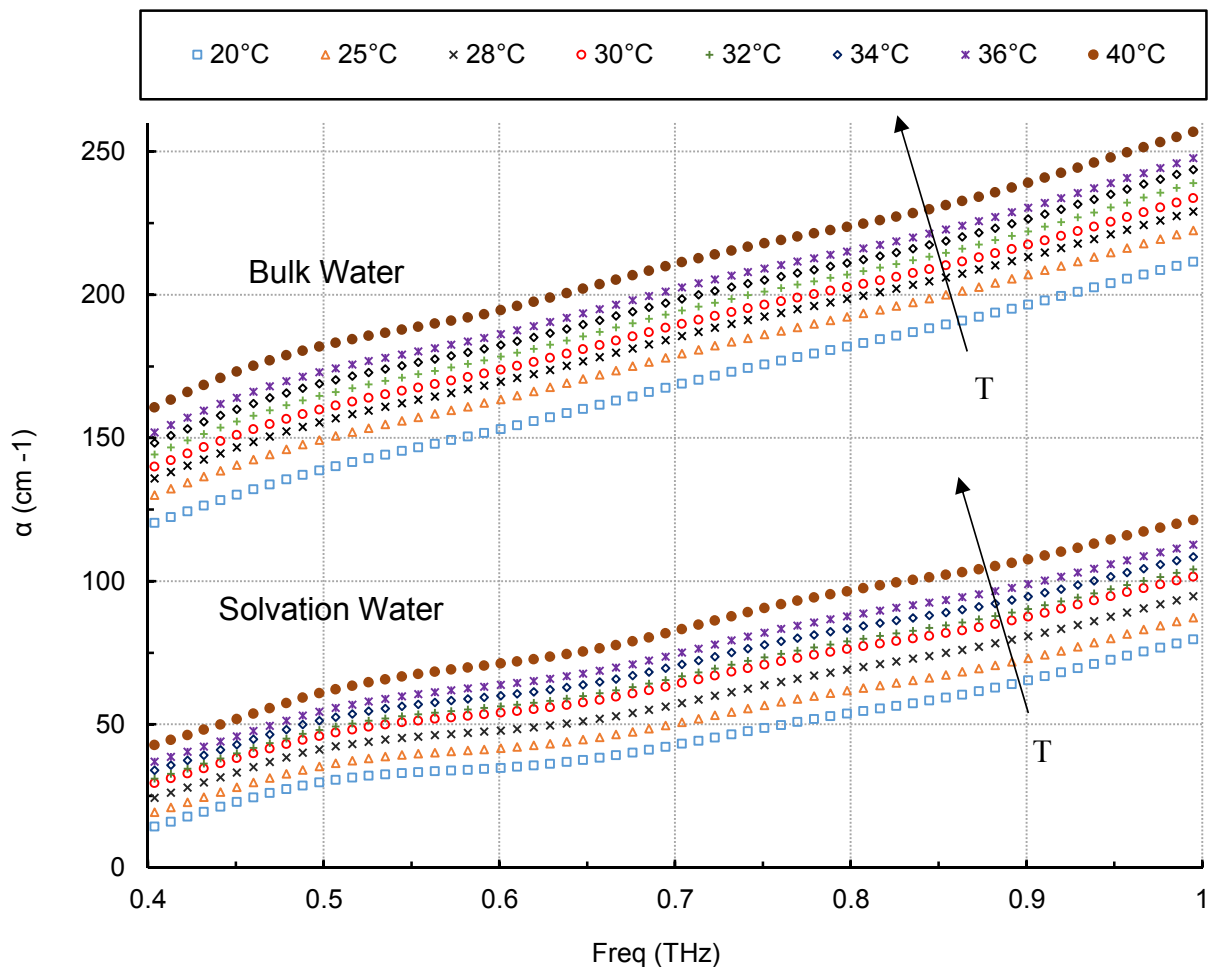


**Figure S13** Absorption coefficient of the solvation water bounded to P7k polymer for sample P7K15, based on calculation for  $T=20$  to  $28$  °C with  $N_h=11$ , and extrapolated for  $T=30$  to  $40$ °C. Bulk water data are also plotted for comparison.

## S6. EXTRACTION OF THE COIL-TO-GLOBULE $r(T)$ WITH NUMERICAL METHOD $r(T)$

### S6.1. Vant'Hoff plots

We analyzed the work of Hou et al.<sup>7</sup>, where the coil to globule equilibrium constant  $K$  can be estimated from the PNIPAm infrared data (figure 6 of reference 7). The hydrated  $\text{CH}_3$  absorbs at  $2991\text{cm}^{-1}$  while dehydrated  $\text{CH}_3$  absorbs at  $2972\text{cm}^{-1}$ . Observation of an intermediate value  $f(\text{obs})$  corresponds to a mixture of hydrated coil (hereafter “2991”) and dehydrated (“2972”) globule in variable proportions  $p$ . Therefore:

$$f(\text{obs}) = p \cdot 2991 + (1-p) \cdot 2972 \quad (\text{S6.1})$$

And

$$K = \frac{p}{1-p} = \frac{f(\text{obs}) - 2972}{2991 - f(\text{obs})} \quad (\text{S6.2})$$

Vant'Hoff plots are based on:

$$\Delta H^0 - T\Delta S^0 = -RT \cdot \ln K \quad (\text{S6.3})$$

$$i.e. \ln K = \frac{-\Delta H^0}{RT} + \frac{\Delta S^0}{R} \quad (\text{S6.4})$$

Where  $\Delta H^0$  is the standard enthalpy of the reaction,  $S$  is the entropy,  $R$  is the gas constant,  $T$  is the temperature and  $K$  is the equilibrium constant. Here, the equilibrium constant  $K$  needs to be known.

Then, plotting  $\ln K$  vs.  $1/T$  gives  $-\Delta H^0/R$  as slope and  $\Delta S^0/R$  as intercept. Figure S14 has been obtained by considering the seven temperatures around the LCST.

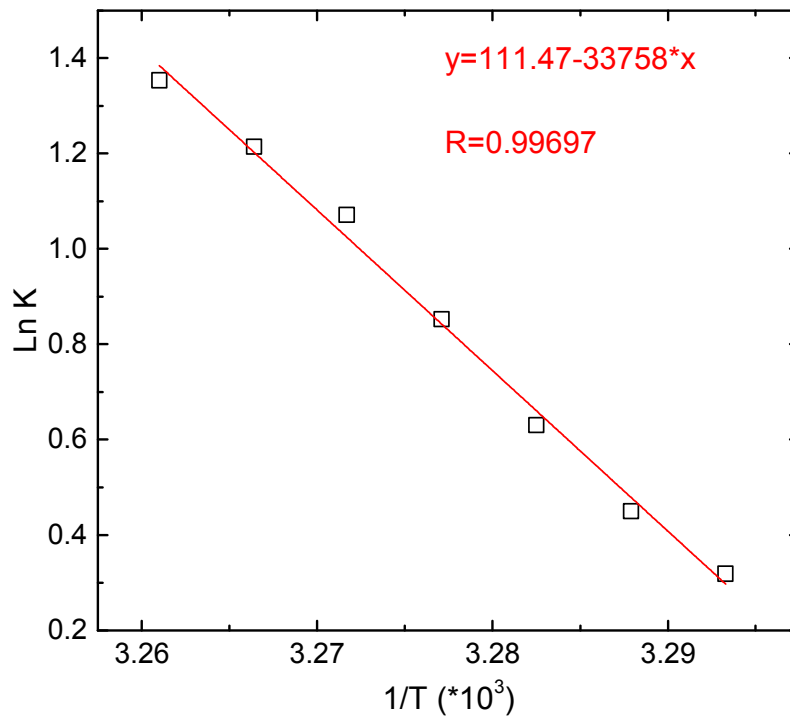


**Figure S14:** Vant'Hoff plots obtained from data of figure 6 (PNIPAm) in ref. 7.

We found  $\Delta H^0 / R = 33758 \text{ K}$  and  $\Delta S^0 / R = 111.5$ , The critical temperature  $T^*$  where  $[\text{coil}] = [\text{globule}]$  (i.e.  $K(T^*) = 1$  or  $\Delta G^0(T^*) = 0$ ) is then  $33758 / 111.5 = 303 \text{ K}$ .

Knowing that the PNIPAm used in ref. 7 has a molar mass  $M_w = 12 \text{ kg} \cdot \text{mol}^{-1}$ , the enthalpy in  $\text{J} \cdot \text{g}^{-1}$  is about:  $33758 \cdot 8.31 / 12000 = 23.4 \text{ J} \cdot \text{g}^{-1}$ .

## S6.2. r(T) formula

To analyze sigmoidal curves, we used r(T) formula<sup>8</sup>, which is a variant of the Vant'Hoff formula but it does not necessitate the previous knowledge of the equilibrium constant K.

Formula r(T) has been developed for  $A \leftarrow \rightarrow B$  thermochromic equilibria. It allows the estimation of the thermodynamic parameters  $\Delta H^0/R = h$  (in K units) and  $\Delta S^0/R = s$  (adimensional) from the sole shape analysis of the variation of a colligative property of the equilibrium vs. T.

For instance,

$$Y = Y_a(a) + Y_b(b) \quad (\text{S6.2.5})$$

Where Y is the colligative property,  $Y_a$  and  $Y_b$  are the sensitivities of A and B respectively for this property and a and b are the molar fractions of A and B respectively, thus  $a + b = 1$ .

Since  $Y_a$  and  $Y_b$  are unknown, a and b remain also unknown and the equilibrium constant  $K = b/a$  cannot be obtained directly from Y. Combining Y and K gives:

$$Y = \frac{Y_a + KY_b}{1+K} \quad (\text{S6.2.6})$$

$$K = e^{-\frac{h}{T} + s} = e^{-\frac{h}{T}} e^s \quad (\text{S6.2.7})$$

In order to cancel the scale factors  $Y_a$  and  $Y_b$  to keep only the thermodynamic parameters h and s, the first and the second derivatives must be calculated.

- Calculation of the first derivative:

$$\frac{dY}{dT} = \frac{dY}{dK} \frac{dK}{dT} \quad (\text{S6.2.8})$$

The second term of the product on the right side is the Van't Hoff law:

$$\frac{dK}{dT} = \frac{h}{T^2} K \quad (\text{S6.2.9})$$

The first term gives from S6.2.6, with  $\Delta Y = Y_a - Y_b$

$$\frac{dY}{dK} = \frac{Y_b - Y_a}{(1+K)^2} = - \frac{\Delta Y}{(1+K)^2} \quad (\text{S6.2.10})$$

Therefore,

$$\frac{dY}{dT} = - \frac{\Delta Y \frac{h}{T^2} K}{(1+K)^2} \quad (\text{S6.2.11})$$

- Calculation of the second derivative:

$$\frac{d^2Y}{dT^2} = \frac{dK}{dT} \frac{d}{dT} \left( \frac{dY}{dK} \right) + \frac{dY}{dK} \left( \frac{d^2K}{dT^2} \right) \quad (\text{S6.2.12})$$

With

$$\frac{d}{dT} \left( \frac{dY}{dK} \right) = \frac{2\Delta Y \frac{h}{T^2} K}{(1+K)^3} \quad (\text{S6.2.13})$$

And

$$\frac{d^2K}{dT^2} = \frac{hK}{T^2} \left( \frac{h}{T^2} - \frac{2}{T} \right) \quad (\text{S6.2.14})$$

This leads to

$$\frac{d^2Y}{dT^2} = \left( \frac{\Delta Y \frac{h}{T^2} K}{(1+K)^2} \right) \left( \frac{2hK}{T^2(1+K)} + \frac{2}{T} - \frac{h}{T^2} \right) \quad (\text{S6.2.15})$$

Making the ratio, hereafter called the  $r(T)$  formula, of the second derivative over the first derivative eliminates the scaling factor  $\Delta Y$ :

$$r(T) = \frac{\frac{d^2Y}{dT^2}}{\frac{dY}{dT}} = \frac{h}{T^2} \frac{(1-K)}{(1+K)} - \frac{2}{T} \quad (\text{S6.2.16})$$

Expression of K (equation S6.7) shows that  $r(T)$  contains only two parameters:  $h = \Delta H^0/R$  and  $s = \Delta S^0/R$ , which estimation leads to a model to fit the experimental data (figure S15).

Analysis of PNIPAm THz-TDS experimental data by  $r(T)$  formula :

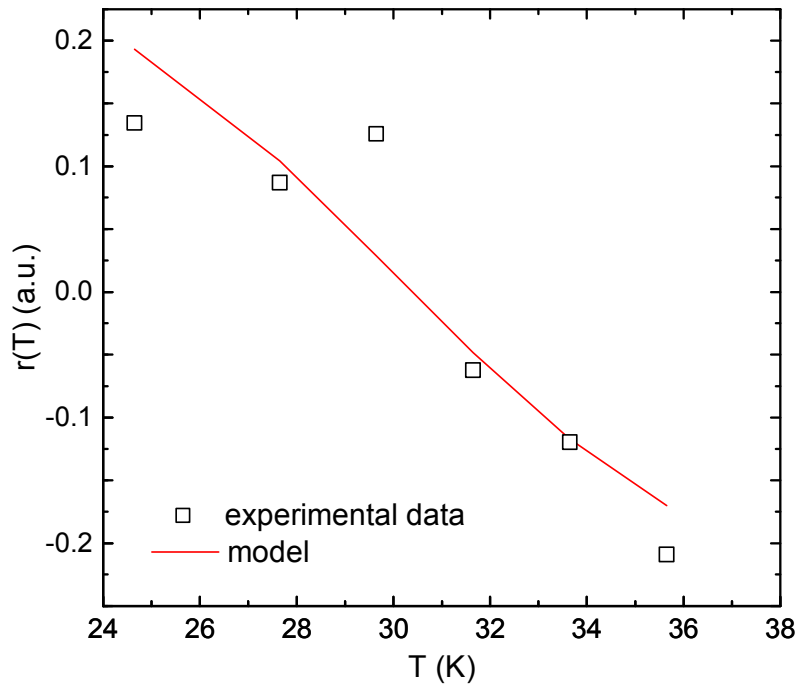


**Figure S15:**  $r(T)$  used on experimental data for sample P7K15 at 0.8 THz. Dots: experimental  $r(T)$  values from successive numerical derivation; solid line :  $r(T)$  algebraic formula plotted with estimated values  $\Delta H^0/R = 25843$  K and  $\Delta S^0/R = 85$ .

The estimation of the  $\alpha_1$  and  $\alpha_2$  scaling factors is reached when  $K \rightarrow \infty$  and  $K \rightarrow 0$  respectively, as  $\alpha = (\alpha_1 - \alpha_2)p + \alpha_2$  and  $p = K/(1+K)$ . With  $K = (\exp(-\Delta H^0/RT)) * (\exp(\Delta S^0/R))$ , plotting of  $\alpha$  vs.  $p$  for all values of  $p$  gives a straight line whose intercept is  $\alpha_2$  and slope is  $(\alpha_1 - \alpha_2)$  (Fig S16).

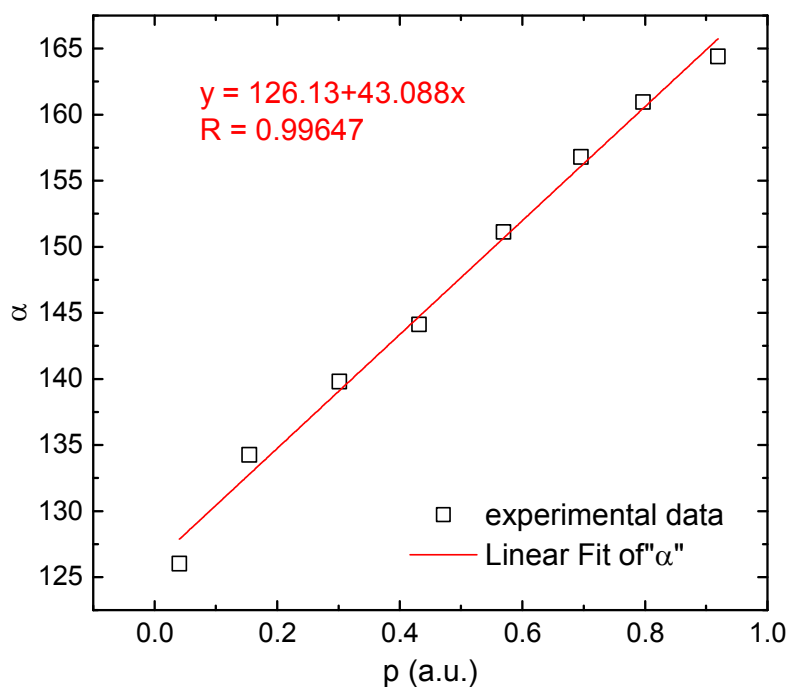


**Figure S16:** Estimation of the scaling factors at 0.8THz for a sample P7K15;  $\alpha_1 = 169$  and  $\alpha_2 = 126$ .

Re-analysis of Hou's results (ref. 7) from  $r(T)$  formula (*i.e.* ignoring the scale of the diagram considering only its sigmoidal shape) gives after smoothing  $\Delta H^0/R = 43000$  K and  $\Delta S^0/R = 142$  ( $T_c = 303$ K) *i.e.*  $29.8 \text{ J.g}^{-1}$  for the enthalpy. Depending on the data treatment technique the Hou's enthalpy is estimated at:  $27 \pm 3 \text{ J.g}^{-1}$ .

## S7. SUPPLEMENTARY REFERENCES

- (1) Naftaly, M.; Miles, R. E. Terahertz Time-Domain Spectroscopy for Material Characterization. *Proc. IEEE* **2007**, *95* (8), 1658–1665.
- (2) Vij, J. K.; Hufnagel, F. Millimeter and Submillimeter Laser Spectroscopy of Water. *Chem. Phys. Lett.* **1989**, *155*, 153–156.
- (3) Hasted, J. B.; Husain, S. K.; Frescura, F. A. M.; Birch, J. R. Far-Infrared Absorption in Liquid Water. *Chem. Phys. Lett.* **1985**, *118*, 622–625.
- (4) Thrane, L.; Jacobsen, R. H.; Uhd Jepsen, P.; Keiding, S. R. THz Reflection Spectroscopy of Liquid Water. *Chem. Phys. Lett.* **1995**, *240*, 330–333.
- (5) Kindt, J. T.; Schmuttenmaer, C. A. Far-Infrared Dielectric Properties of Polar Liquids Probed by Femtosecond Terahertz Pulse Spectroscopy. *J. Phys. Chem.* **1996**, *100*, 10373–10379.
- (6) Rønne, C.; Thrane, L.; Åstrand, P.-O.; Wallqvist, A.; Mikkelsen, K. V.; Keiding, S. R. Investigation of the Temperature Dependence of Dielectric Relaxation in Liquid Water by THz Reflection Spectroscopy and Molecular Dynamics Simulation. *J. Chem. Phys.* **1997**, *107*, 5319–5331.
- (7) Hou, L.; Wu, P. Comparison of LCST-Transitions of Homopolymer Mixture, Diblock and Statistical Copolymers of NIPAM and VCL in Water. *Soft Matter* **2015**, *11*, 2771–2781.
- (8) Tan-Sien-Hee, L.; Lavabre, D.; Levy, G.; Micheau, J. C. Multiwavelength Analysis of Thermo-chromic Equilibria Application to the [Ni (tmen) (acac)]<sup>+</sup> Ion in Different Solvents. *New J. Chem.* **1989**, *13*, 227–233.